Mathematics-Based Modeling of a Series-Hybrid Electric Vehicle

Thanh-Son Dao, Aden Seaman, John McPhee
University of Waterloo
Waterloo, ON, N2L 3G1, Canada
Emails: tsdao@engmail.uwaterloo.ca,
anseaman@real.uwaterloo.ca,
mcphee@real.uwaterloo.ca

ABSTRACT

The recent increase in oil price and environmental concerns has attracted various research efforts on hybrid electric vehicles (HEVs) which provide promising alternatives to conventional engine-powered vehicles with better fuel economy and fewer emissions. To speed up the design and prototyping processes of new HEVs, a method that automatically generates mathematics equations governing the vehicle system response in an optimized symbolic form is desirable.

To achieve this goal, we employed MapleSim^{TM} 4.0, a new physical modeling tool developed by Maplesoft Inc., to develop the multi-domain model of a series-HEV, utilizing the symbolic computing algorithms of Maple software package to generate an optimized set of governing equations. The HEV model consists of a mean-value internal combustion engine (ICE), a chemistry-based Ni-MH battery pack, and a multibody vehicle model.

Simulations are then used to demonstrate the performance of the developed HEV system. Simulation results show that the model is viable and the number of governing equations is reduced significantly, resulting in a computationally efficient system.

1. INTRODUCTION

In recent years, a significant amount of research has focused on HEVs due to environmental pressure to achieve better fuel economy and cleaner vehicles than conventional cars (Butler *et al*., 1999, Baumann *et al*., 2000, MacBain *et al*., 2003, Wei *et al*., 2006, Simpson *et al*., 2009). Since the first global-scale commercialization of the hybrid passenger vehicle Toyota Prius in 1997 and then Honda Insight in 1999, the production and sales of HEVs has been increasing rapidly, mainly due to the worldwide increase in oil prices. The development of new HEVs is now considered as the top priority by most major automakers. The advantages of HEVs include lower emissions, better fuel economy, longer distances between re-fueling, and higher efficiency.

In the competitive automotive market, car makers are under pressure to design and build cars faster. Therefore, a computationally efficient mathematical HEV model is necessary to accelerate the design process. To achieve this objective, the model should be created in a symbolic form which can easily be viewed and shared among engineers, who can alter the codes or enter their own math-based components into the model. The symbolic form facilitates sensitivity analysis and design optimization, as well as real-time simulation.

In the design and development of HEVs, modeling engineers also face many other challenges since the modeling of an HEV covers many different physical domains, among which are mechanical, electrical, thermal, hydraulic, and chemical domains. With that in mind, we use Maplesoft's new mathematic-based modeling tool MapleSim, built upon the Maple symbolic computing system, to develop the symbolic model of a HEV. This HEV model consists of a controller to control vehicle and battery states, a mean-value ICE, an electric generator powered by the ICE, a Ni-MH battery pack, a DC motor/generator, and a 3D vehicle multibody dynamic model. Existing HEV models typically neglect the 3D multibody dynamics of vehicles, instead representing them as particle masses with simple rolling resistance and aerodynamic drag (Butler *et al*., 1999, Baumann *et al*., 2000, MacBain *et al*., 2003, Wei *et al*., 2006, Simpson *et al*., 2009). Given the significant contributions of tires and suspensions to power losses, it is important to have a higher-fidelity multibody vehicle model within the HEV system model. Modeling the HEV in MapleSim allows the model to be transformed into optimized code that can be used for sensitivity analysis, model reduction, and real-time applications such as hardware-in-the-loop (HIL) simulations.

Depending on the way power is supplied to the drivetrain, HEVs can be classified into the following three main architectures:

- **Parallel hybrid** in which the ICE and DC motor are simultaneously connected to a mechanical transmission (Salman *et al*., 2000, Won *et al*., 2005, Lin *et al*., 2003), allowing the wheels to be turned by two mechanically coupled sources of power. Although this architecture provides economic gain due to the use of a small traction motor, it also

contains a complicated control system which requires a higher maintenance cost and has a higher potential to break-down if control algorithms are not carefully designed. The 2010 Honda's Insight, Civic, Accord and 2005 Ford Escape SUV are examples of production parallel hybrids.

- **Series hybrid** in which the wheels are rotated only by traction motors which are powered by a battery pack. The ICE is only used to charge the battery when required (Powell and Pilutti, 1995, Brahma *et al*., 2000). This architecture is usually referred to as a fully electric or "range-extender" vehicle with an ICE assist. Although a series-HEV usually requires a larger traction drive system since all the power needed to move the vehicle has to pass through the generator and motor, it has many advantages, including better fuel efficiency, optimized efficient power plant, small space packaging, and long operation life. Examples of series-HEV include the 2010 Chevrolet Volt and Daimler AG's Orion bus.
- **Power-split hybrid** which combines both parallel and series hybrid architectures (Kimura *et al*., 1999, Rizoulis *et al*., 2001, Liu and Peng, 2008). This architecture is more efficient overall, but at the cost of more complicated control systems. Several vehicles of this type include Toyota's Prius and Lexus RX400h, Ford's Escape, and Nissan's Altima.

In this paper, the series-hybrid form is studied due to simple architecture and advantages over other forms of hybrid. The paper is organized as follows: Section 2 details the components used in the HEV model. This includes the formulations for the ICE, Ni-MH battery, power converter, vehicle dynamics, and tire model. Section 3 discusses the use of MapleSim and Maple language to develop the HEV model and generate the optimized code of the system equations. Section 4 provides simulation results to validate the proposed model. Finally, some concluding remarks are given in Section 5.

2. SERIES-HEV MODEL ARCHITECTURE

The series-HEV model presented in this paper is illustrated in Fig. 1. The mathematics-based modeling of HEVs is complex because it requires the associations of devices in different domains with very different dynamics and characteristics. The vehicle uses an ICE to generate power for an electric generator which, in turn, converts mechanical work into electricity to charge a Ni-MH battery pack whenever the battery state of charge (SOC) drops below a minimum charge level. A power controller is used to determine how much current to be drawn from the battery in order to turn the wheels according to the speed requirement. When the driver reduces vehicle speed by stepping on the brake pedal, the DC motors are put into the

reverse mode and act as electric generators to charge the battery pack. Details about each component in the HEV model are presented in the following subsections
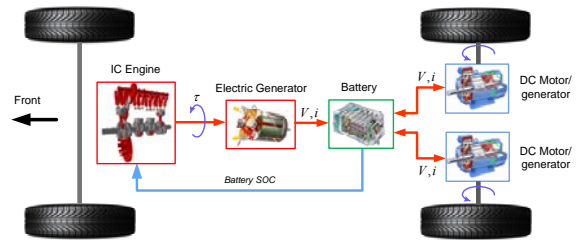

Figure 1. SERIES-HYBRID ELECTRIC VEHICLE MODEL.

2.1 Mean-Value ICE Model

In this work, the mean-value engine model developed by Saeedi (2010) has been used since this model is computationally efficient while capturing enough information about the physics of the engine system.

The mathematic equations describing the engine model have been given by Moskwa (1988), Heywood (1988), Crossley and Cook (1991), and Hendricks *et al.* (1996). The engine model is composed of three main subsystems: the throttle, intake manifold, and engine power generation from the fuel combustion. The rate of air mass flowing into the engine is determined based on the geometry and position of the throttle valve set by a simple PID controller which closes the loop between the actual and desired engine speeds. The intake manifold has a significant effect on the gas flow and pressure to the engine cylinders. The pressure of the air/fuel mixture in the intake manifold can be calculated based on the ideal gas equation:

$$\dot{P}_m = \frac{RT_m}{V_m}\left(\dot{m}_{thr} - \dot{m}_e\right) \qquad (1)$$

where R is the gas constant, T_m and V_m are the temperature and volume of the intake manifold, $\dot{m}_{thr}$ is the throttle mass flow rate, and $\dot{m}_e$ is the throttle mass outflow.

The calculated air/fuel pressure and mass flow rate in the manifold are used to compute the power generated from the engine through the combustion of the fuel in the gas mixture delivered to the cylinders, accounting for thermal efficiency, friction, and inertial losses in the engine and the inertial load at the drive shaft. The engine power is calculated based on the engine equations proposed by Hendricks (1996):

$$P_{net} = P_{ind} - P_{loss} - P_{load} \qquad (2)$$

where P_{ind}, P_{loss}, and P_{load} are the indicated power, lost power, and load power, respectively.

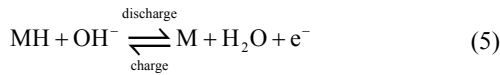The engine speed can be obtained from crank shaft speed equation as:

$$\dot{n} = \frac{1}{J_e n} P_{net} \qquad (3)$$

where J_e is engine inertia and n is the engine rotational speed.

2.2 Chemistry-Based Ni-MH Battery Model

There are currently several different approaches for car battery modeling, the most popular of which can be categorized into: (1) Circuit-based approach in which battery behaviors are presented as an electrical circuit (Salameh *et al.*, 1992, Chen and Rinćon-Mora, 2006). The circuit-based approach results in a conceptually simple model. However, the actual physical parameters are hidden and there is no explicit relationship between the model parameters and battery parameters, making remodeling difficult as a different battery is used. (2) Chemistry-based approach that captures the actual chemical reactions and other electrochemical processes in a battery. The chemistry-based approach can be seen in the works done by Newman *et al.*, (1997, 2004, 2008) and Wu *et al.* (2001). In this paper, the chemistry-based approach allows us to vary battery physical parameters for the design and control purposes to match the requirements for the HEV.

Due to its dominance in almost all hybrid vehicles, a Ni-MH battery has been chosen for the HEV model in this paper. The Ni-MH battery model presented is a modified version of the battery model proposed by Wu *et al.* (2001). For simplicity, the effects of side chemical reactions and thermal effects have been ignored. The two main chemical reactions on the two electrodes of the battery are:

$$\text{NiOOH} + \text{H}_2\text{O} + \text{e}^- \underset{\text{charge}}{\overset{\text{discharge}}{\rightleftharpoons}} \text{Ni(OH)}_2 + \text{OH}^- \qquad (4)$$

$$\text{MH} + \text{OH}^- \underset{\text{charge}}{\overset{\text{discharge}}{\rightleftharpoons}} \text{M} + \text{H}_2\text{O} + \text{e}^- \qquad (5)$$

where the metal M in the negative electrode is an inter-metallic compound, usually a rare earth compound.

The electromotive force in the battery is defined by the two open-circuit voltage equations (*i.e.*, Nernst equations) for cathode and anode:

$$\phi_c = U_{pos} + (T - T_0)\frac{\partial U_{pos}}{\partial T} + \frac{RT}{F}\ln\left(\frac{c_{\text{H}^+,\text{max}} - c_{\text{H}^+}}{c_e c_{\text{H}^+}}\right) \qquad (6)$$

$$\phi_a = U_{neg} + (T - T_0)\frac{\partial U_{neg}}{\partial T} + \frac{RT}{F}\ln c_e + 9.712\times10^{-4}$$
$$+0.23724e^{-\frac{28.057 c_{\text{MH}}}{c_{\text{MH,max}}}} - \frac{2.7302\times10^{-4}}{\left(c_{\text{MH}}/c_{\text{MH,max}}\right)^2 + 0.010768} \qquad (7)$$

In these equations, c_{H^+} and $c_{\text{H}^+,\text{max}}$ are the current and maximum concentrations of Ni(OH)_2; c_{MH} and $c_{\text{MH,max}}$ are the current and maximum concentrations of MH; c_e is the concentration of the KOH electrolyte; U_{pos} and U_{neg} are the standard open-circuit potentials on cathode and anode, respectively.

The rate of chemical reaction on each electrode is defined by the Butler-Volmer equation which relates the current density j_i to the over-voltage η_i by:

$$j_i = i_{0,i}\left(e^{\frac{0.5F}{RT}\eta_i} - e^{\frac{-0.5F}{RT}\eta_i}\right) \qquad (8)$$

where i = pos (positive) for cathode and i = neg (negative) for anode, F is the Faraday constant, R is the gas constant, T is the battery temperature, and $i_{0,i}$ is the exchange current density given by:

$$i_{0,i} = i_{0,i,\text{ref}}\left(\frac{c_i}{c_{i,\text{ref}}}\right)^{0.5}\left(\frac{c_e}{c_{e,\text{ref}}}\right)^{0.5}\left(\frac{c_{i,\text{max}} - c_i}{c_{i,\text{max}} - c_{i,\text{ref}}}\right)^{0.5} \qquad (9)$$

where $c_i = c_{\text{H}^+}$ for cathode and $c_i = c_{\text{MH}}$ for anode, and $i_{0,i,\text{ref}}$ is the exchange current density at a reference reactant concentration.

The battery cell current i_{cell} can be calculated from the charge balance equations on the electrodes given by:

$$i_{\text{cell}} = A_i a_i l_i j_i \qquad (10)$$

where A_i, a_i, and l_i are the total geometry area, the specific surface area, and the thickness of the electrode, respectively.

The cell voltage is given by:

$$v_{\text{cell}} = (\phi_c + \eta_c) - (\phi_a + \eta_a) + i_{\text{cell}} R_{\text{int}} \qquad (11)$$

where R_{int} is the ohmic internal resistance of the cell.

The parameters used for the battery model were measured from a 4.5 *Ah* VARTA Ni-MH battery at the Ford Motor Company Scientific Research Laboratory (see Wu *et al.*, 2001) and are listed in Table 1.
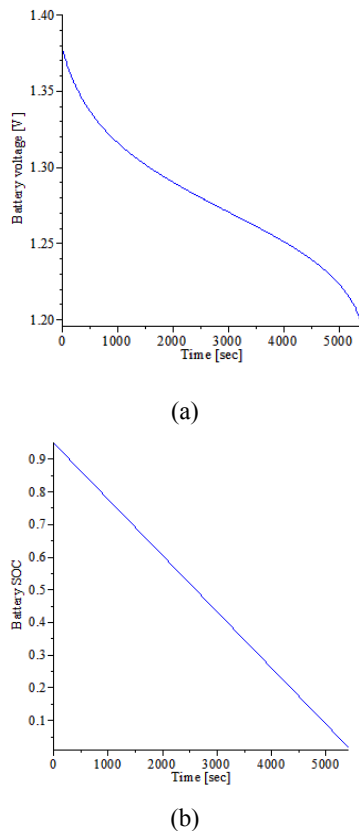
(a)

(b)

Figure 2. (a) BATTERY VOLTAGE AND (b) SOC WHEN
DISCHARGED WITH CONSTANT CURRENT OF 4A.

2.3 Power Controller

In order to control the amount of power going from the battery to the motor during driving, or vice-versa during regenerative braking, a power controller is necessary. If the battery's voltage needs to be stepped-up to operate the motor, a boost converter is used. If the voltage needs to be stepped-down, then a buck converter is used (see Bauman, 2008). Both types of converters use non-linear electrical circuits with variable-duty high frequency switching transistors to convert one DC voltage level to another.

Instead of modeling the full high-frequency circuit in MapleSim, we used a simple approximation that considers the power controller's steady-state behaviour, and can be used as either as boost or a buck converter (see Figure 3). Our approximate model allows the user to determine what current flows in the output loop. The output loop's voltage at this current level is measured and the output power is calculated. The input power is calculated in the same way, but a PID controller adjusts the input loop current until the input power equals the output power. This technique works both for positive and negative currents, allowing the model to be used for discharging and charging

of the battery. Furthermore it works for varying voltage and impedance conditions of the battery and motor, and works when the output current and voltage go to zero, avoiding any algebraic singularities.

This simple model assumes 100% efficiency of the power electronics, but a more realistic efficiency model such as the one used by Hellgren (2002) can be incorporated. Also, it does not take into consideration the physical limitations of the components of the system.
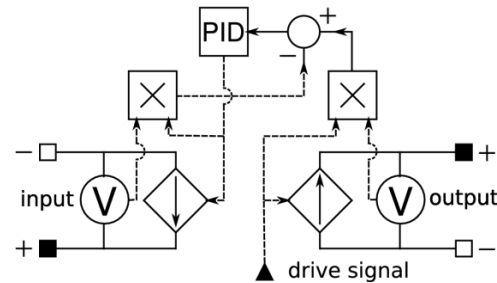

Figure 3. BLOCK DIAGRAM OF POWER CONTROLLER.

2.4 Vehicle Dynamics

The vehicle is represented as a generic four-wheeled vehicle model with independent one-DOF suspensions (see Fig. 4). This model is sufficient to predict the handling and braking behaviors of an automobile without the effort of modeling all of the small details such as bushings, linkage properties, etc. The model has fourteen DOFs: six DOFs of the chassis, four DOFs for the four unsprung masses in the vertical direction, and four spin DOFs for the wheels. The vehicle body is modeled as a rigid with body fixed coordinates xyz attached at the centre of gravity G and aligned in principal directions. The position of the body with respect to the inertial frame XYZ can be determined through the 1-2-3 Euler angles (*i.e.*, the roll angle φ, the pitch angle θ, and the yaw angle ψ).

The forces and moments acting on the tire models are resolved in the ISO tire axis system with the three unit vectors being $\mathbf{u}_x$ (pointing forward in the direction of wheel heading), $\mathbf{u}_y$ (lateral direction of the tire), and $\mathbf{u}_z$ (normal to the road surface). The forces and moments acting at the tire/ground contact patch are the longitudinal force F_x and overturning moment in the ISO X direction, the lateral force F_y and rolling resistance moment in the ISO Y direction, and the normal force F_z and aligning moment M_z in the ISO Z direction as shown in Fig. 5.

The vehicle model uses the Magic Formula developed by Pacejka (2002) to model the tire/contact patch interaction and relaxation lengths to model the tire transients. The longitudinal slip and lateral slip used in the tire model were calculated as follows:

$$S = \frac{\Omega R_{eff} - V_{Cx}}{|V_{Cx}|} = \frac{\Omega R_{eff} - \mathbf{v}_c . \mathbf{u}_x}{|\mathbf{v}_c . \mathbf{u}_x|} \qquad (12)$$

$$\alpha = \tan^{-1}\left(\frac{V_{Py}}{|V_{Cx}|}\right) \qquad (13)$$

where V_{Cx} is the tire forward speed (*i.e.*, the *x*-component of the tire center velocity $\mathbf{v}_c$ in ISO axis system) and R_{eff} is the tire effective rolling radius.
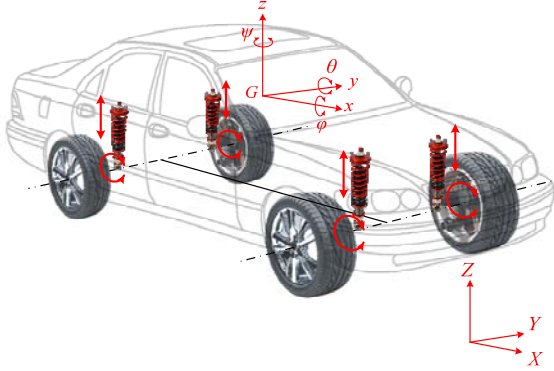

Figure 4. VEHICLE MODEL.

The relaxation lengths used in the model are determined from the formulation proposed by Bernard and Clover (1995) as shown in Eqs. 14 and 15. In this work, the notation B_{long} is the longitudinal relaxation length and B_{lat} is the lateral relaxation length:

$$\frac{\mathrm{d}S}{\mathrm{d}t} = \frac{\Omega R_{eff} - V_{Cx}}{B_{long}} - \frac{S|V_{Cx}|}{B_{long}} \qquad (14)$$

$$\frac{\mathrm{d}\tan(\alpha)}{\mathrm{d}t} = \frac{V_{Py}}{B_{lat}} - \frac{\tan(\alpha)|V_{Px}|}{B_{lat}} \qquad (15)$$

The tire forces at the tire/ground contact point P are then moved to the tire centre C, a well-defined point in the multibody model, using the statics relationships:

$$\mathbf{F}_c = \mathbf{F}_P \qquad (16)$$

$$\mathbf{M}_C = \mathbf{M}_P + \mathbf{r}_{P/C} \times \mathbf{F}_P \qquad (17)$$

The tire/ground contact vector $\mathbf{r}_{P/C}$ is estimated by assuming the tire as a planar disk with variable radius proposed by Postiau *et al.* (2000).

To account for the tire lift-off when the tire compression becomes less than zero, the tire normal force F_z is set equal to zero and the instantaneous tire radius is considered equal to the nominal tire radius until the tire returns to the road surface:

$$F_z = \max\left(k_z\delta + c_z\dot{\delta}, 0\right) \qquad (18)$$

where δ represents the tire penetration into the ground, k_z is the spring constant, and c_z is the damping coefficient.
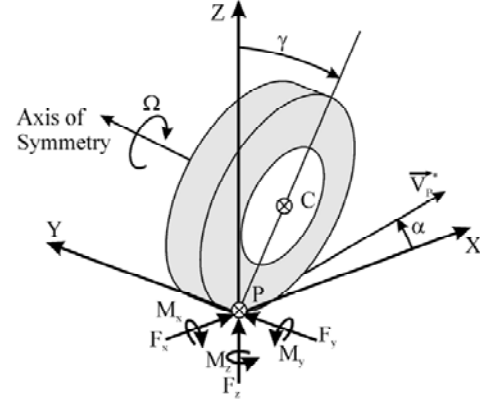

Figure 5. ISO TIRE AXIS SYSTEM.

3. MAPLESIM HEV MODEL

The HEV components consisting of an ICE, a battery pack, controllers, a multibody vehicle, and a motor/generator are developed in MapleSim which is built on top of Maple engine and, hence, inherits the strength of symbolic computation from the Maple language.

The vehicle and tire models are formulated using the graph-theoretical method developed by McPhee *et al.* (1996, 2004, 2008). This results in a compact and efficient set of system equations. The entire system equations are organized into a set of DAEs across multiple domains, namely mechanical domain (vehicle, tire, motor, generator), electrical domain (motor, generator, power converter), chemical domain (battery), and hydraulic domain (ICE) as:

$$\mathbf{M}\dot{\mathbf{p}} + \mathbf{C}^T\mathbf{f} = \mathbf{b}(\mathbf{q}, \mathbf{p}, t) \qquad (19)$$

$$\mathbf{\Phi}(\mathbf{q}, t) = \mathbf{0} \qquad (20)$$

$$\dot{\mathbf{q}} = \mathbf{h}(\mathbf{p}, \mathbf{q}, t) \qquad (21)$$

Equation (19) contains differential equations involving the generalized speeds $\dot{\mathbf{p}}$. The matrix $\mathbf{M}$ contains the coefficients of $\dot{\mathbf{p}}$ in the system's dynamic equations. The portion of $\mathbf{M}$ that corresponds to mechanical variables may be thought of as a mass matrix, whereas the portion corresponds to electrical variables may be thought of as an inductance/capacitance matrix, and electrochemistry coefficients for chemical variables. The column matrix $\mathbf{f}$ contains variables related to the system's constraint equations in the form of constraint forces and the matrix

C gives the coefficients of **f** in the dynamic equations. Equation (20) contains algebraic constraint equations involving the zeroth-level derivative modeling variables **q**. Equation (21) describes kinematic transforms relating the derivatives of the coordinates **q̇** to the generalized speeds **p**, coordinates **q**, and time *t*.

The system equations are then further simplified and optimized using index reduction techniques in MapleSim to reduce simulation time. Maple has the ability to identify repeated terms within the equations and store them as temporary variables allowing them to only have to be evaluated once and used several times.

4. SIMULATIONS

The simulations have been executed in MapleSim. As previously mentioned, MapleSim uses linear graph theory to formulate the governing equations for the vehicle and tire models. Maple's CodeGeneration package is used automatically by MapleSim to optimize the expressions. The original number of equations for the whole HEV system is 605 which are then reduced to 41 equations using simplification and index reduction techniques.

In all simulation scenarios, the Rosenbrock stiff solver is used with the absolute and relative tolerances of 1.0×10^{-4}. Lists of parameters used in the simulations are given in Appendix A. The initial vehicle speed of 15 *m/s* and the initial battery SOC of 80% are used in the simulations. The ICE uses the MapleSim default values for initialization. The other initial conditions are automatically computed by MapleSim.

In the first test, the vehicle is controlled to follow a speed profile shown in Fig. 6. The durations of acceleration and deceleration are both 20 *s*. Since the initial speed is 15 *m/s*, the vehicle has to slow down first and put the DC motor into the reverse mode, charging the battery due to the regenerative braking effort and causing the battery SOC to rise from 80% to the high 85% as seen in Fig. 7. As the vehicle accelerates between 20 *s* and 40 *s*, the battery SOC is heading down as the battery is discharged. When the vehicle speed reaches the peak speed of 20 *m/s*, it travels at this constant speed between 40 *s* and 60 *s*. The power required to overcome friction causes the battery to be discharged again, but at a slower rate. Then battery is charged due to the regenerative braking effort as the vehicle reduces its speed from 20 *m/s* to 10 *m/s*, and discharged as the vehicle travels at a constant speed until the end of the test. It can also be seen from Fig. 7 that more power is required to move the vehicle at high constant speed than at low constant speed. This results in a steeper slope in the SOC curve between 40 *s* and 60 *s* than between 80 *s* and 120 *s*. The battery current is also plotted in Fig. 8 in which negative current represents a charge effort and positive current represents a discharge effort.
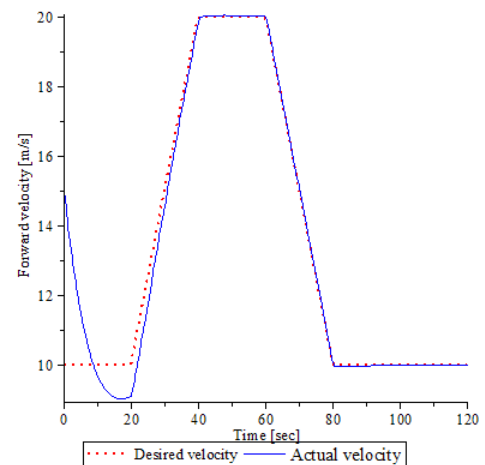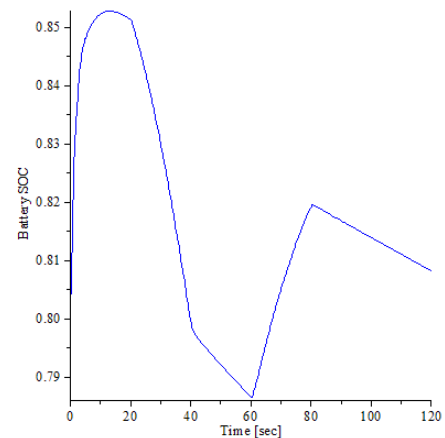

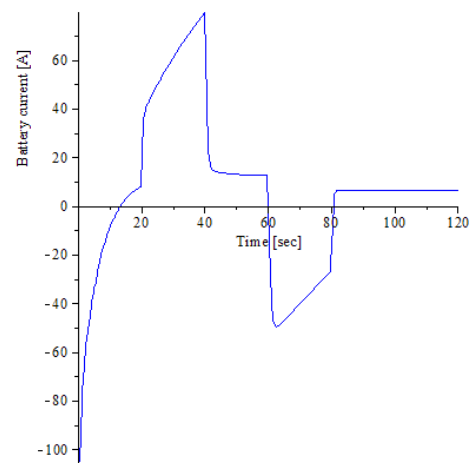Figure 6. VEHICLE SPEED.

Figure 7. BATTERY SOC.

Figure 8. BATTERY CURRENT.

In the second test, the vehicle speed profile (see Fig. 9) is given by the following sinusoidal function:

$$speed = \begin{cases} 8\sin(0.01\pi t)+12 & t \geq 10\ s \\ 12 & t < 10\ s \end{cases} \tag{22}$$

The battery SOC is plotted in Fig. 10, which shows the charge and discharge processes as the vehicle follows the sinusoidal speed function.

A simple on-off controller is used to determine when to close/open the throttle valve of the ICE based on the battery SOC. In this model, the throttle valve is adjusted to only allow minimum air flow into the intake manifold, causing the ICE to rotate at an idle speed of 1000 *rpm* when the battery SOC is higher than a minimum level of 50%. Once the battery SOC drops below this minimum SOC level, the throttle valve is regulated to allow more air flow into the intake manifold, driving the electric generator to charge the battery up to 80%.
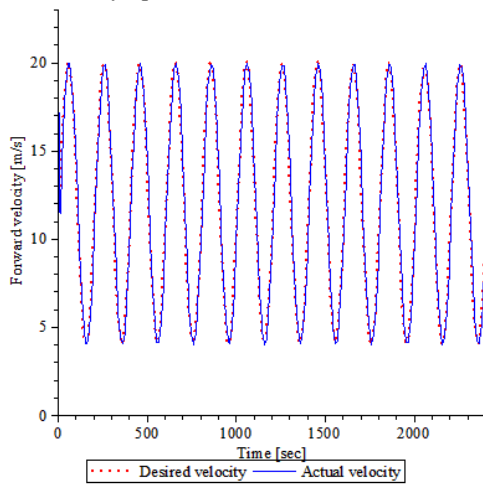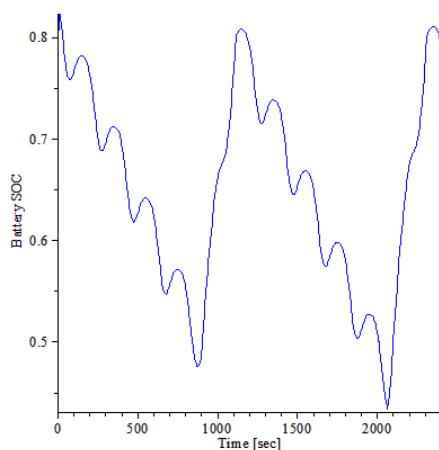

Figure 9. VEHICLE SPEED.

Figure 10. BATTERY SOC.

The position of the throttle valve in degrees during the second test is plotted in Fig. 11. As expected, the vehicle fuel consumption in litres shown in Fig.12 is at minimum when the throttle valve is closed and increases when the valve is open wider. Since the ICE is only turned on to charge the battery pack, the fuel consumption can be reduced significantly compared to conventional vehicles that rely on ICEs as the only source of power, not to mention that the efficiency of a battery-powered vehicle is much higher than that of a vehicle powered only by an ICE (*i.e.*, 80% for batteries versus 20% for ICEs) as shown by Guzzella and Sciarretta (2004).
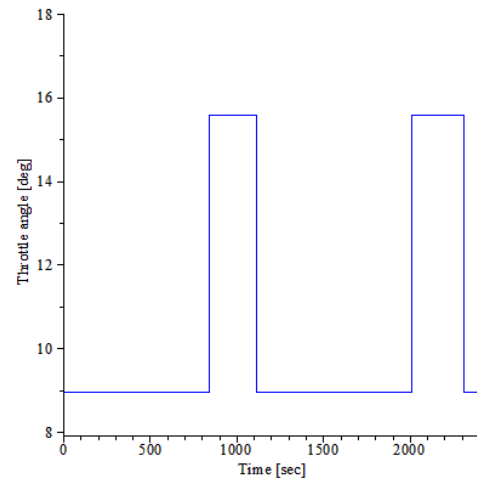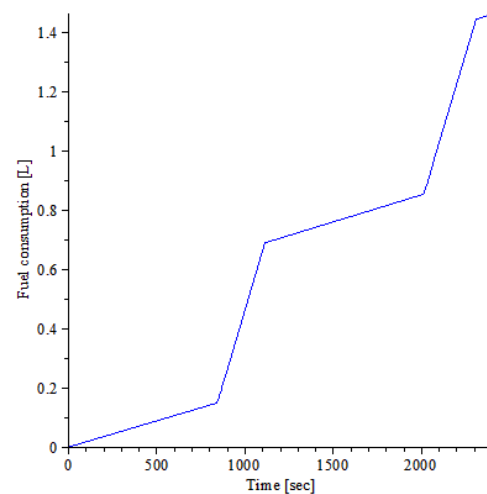

Figure 11. ICE THROTTLE ANGLE.

Figure 12. FUEL CONSUMPTION.

5. CONCLUSION

An approach to modeling a series-HEV based on a mean-value ICE, a chemistry-based Ni-MH battery pack, and a multibody dynamic vehicle has been proposed. This

was accomplished using MapleSim utilizing symbolic operations from a general purpose algebra software package to develop and optimize the system equations. The model contains a set of DAEs across multiple domains, namely mechanical, electrical, chemical, and hydraulic domains.

The simulation results obtained were viable and show that the number of governing equations is reduced significantly, making real-time simulations and HIL applications promising.

One of the main advantages of the approach presented in this paper is that once the model is developed in MapleSim, the system equations can be generated using Maple commands and the code can be exported into other forms and simulated in other environments; as an example, further improvements can be made to the simulation time by compiling the code in C/C++ rather than in Maple's environment.

This HEV model can be used for design, control, and to predict vehicle handling performance under different driving scenarios. The model can also be used for sensitivity analysis, model reduction, and real-time applications such as hardware-in-the-loop (HIL) simulations.

ACKNOWLEDGMENT

REFERENCES

Albertus, P., Christensen, J., and Newman, J., Modeling side reactions and nonisothermal effects in nickel metal-hydride batteries, *Journal of the Electrochemical Society*, Vol. 155, No. 1, pp.A48-A60, 2008.

Bakker, E., Nyborg, L., and Pacejka, H.B., Tyre modeling for use in vehicle dynamic studies, SAE technical paper 870421.

Bauman, J., *Advances in Fuel Cell Vehicle Design*, PhD thesis, University of Waterloo, 2008.

Baumann, B., Washington, G., Glenn, B., and Rizzoni, G., Mechatronics design and control of hybrid electric vehicles, *IEEE/ASME Trans. Mechatron.*, Vol. 5, No. 1, pp.58–72, 2000.

Bernard, J.E. and Clover, C.L., Tire modelling for low-speed and high-speed calculations, SAE technical paper 950311, 1995.

Brahma, A., Guezennec, Y., and Rizzoni, G., Optimal energy management in series hybrid electric vehicle, *Proc. of American Control Conference*, Chicago, 2000.

Butler, K.L., Ehsani, M., and Kamath, P., A Matlab-based modeling and simulation package for electric and hybrid vehicle design, *IEEE Trans. on Vehicular Technology*, Vol. 48, No. 6, 1999.

Chen, M. and Rincón-Mora, G.A., Accurate electrical battery model capable of predicting runtime and i-v performance, *IEEE Trans. On Energy Conversion*, Vol. 21, No. 2, pp.504-511, 2006.

Guzzella, L. and Sciarretta, A., *Vehicle Propulsion Systems: Introduction to Modeling and Optimization*, Springer, 2007.

Hellgren, J., Modelling of hybrid electric vehicles for virtual prototyping, *Proc. of the 2nd International Modelica Conference*, pp.247-356, 2002.

Heywood, J.B., *Internal Combustion Engine Fundamentals*, McGraw Hill, 1988.

Hofman, T. and van Druten, R., Energy analysis of hybrid vehicle powertrains, *Proc. of the IEEE Int. Symposium on Vehicle Power and Propulsion*, Paris, France, 2004.

Kimura, A., Abe, T., and Sasaki, S., Drive force control of a parallel-series hybrid system, *J. SAE Rev.*, Vol. 20, pp.337-341, 1999.

Lin, C.C., Peng, H., Grizzle, J.W., and Kang, J., Power management strategy for a parallel hybrid electric truck, *IEEE Trans. On Control Systems Technology*, Vol. 11, No. 6, pp.839-849, 2003.

Liu, J. and Peng, H., Modeling and control of a power-split hybrid vehicle, *IEEE Trans. On Control Systems Technology*, Vol. 16, No. 6, pp.1242-1251, 2008.

MacBain, J.A., Conover, J., and Brooker, A.D., Full vehicle simulation for series hybrid vehicles, *Future Transportation Technology Conference, SAE-2003-01-2301*, California, 2003.

McPhee, J., On the use of linear graph theory in multibody system dynamics, *Nonlinear Dynamics*, Vol. 9, pp.73-90, 1996.

McPhee, J., Schmitke, C., and Redmond, Dynamic modelling of mechatronic multibody systems with symbolic computing and linear graph theory, *Mathematical and Computer Modelling of Dynamical Systems*, Vol. 10, No. 1, pp.1-23, 2004.

Moskwa, J.J., *Automotive Engine Modeling for Real-Time Control*, Ph.D. Dissertation, Massachusetts Institute of Technology, 1988.

Newman, J. and Thomas-Alyea, K.E., *Electrochemicla Systems*, 3rd ed, John Wiley & Sons Inc., 2004.

Pacejka, H.B., *Tire and Vehicle Dynamics*, Society of Automotive Engineers, Warrendale, PA, 2002.

Paxton, B. and Newman, J., Modeling of nickel/metal hydride batteries, *J. Electrochem. Soc.*, Vol. 144, No. 11, pp.3818-3831, 1997.

Postiau, T., Sass, L., Fisette, P., and Samin, J.C., High-performance multibody models of road vehicles: fully symbolic implementation and parallel computation, *20th International Congress of Theoretical and Applied*

Mechanics, pp.57-83, 2000.

Powell, B.K. and Pilutti, T.E., A range extender hybrid electric vehicle dynamic model, *Proc. of the 33rd Conference on Decision and Control*, Florida, pp. 2736-2741, 1994.

Rizoulis, D., Burl, J., and Beard, J., Control strategies for a series-parallel hybrid electric vehicle, SAE-2001-01-1354, 2001.

Saeedi, M., *A Mean Value Internal Combustion Engine in MapleSim*, MSc thesis, University of Waterloo, 2010.

Salameh, Z.M., Casacca, M.A., and Lynch, W.A., A mathematical model for lead-acid batteries, *IEEE Trans. On Energy Conversion*, Vol. 7, No. 1, pp.93-98, 1992.

Salman, M.A., Schouten N., and Kheir, N.A., Control strategies for parallel hybrid vehicles, *Proc. of the American Control Conference*, pp.524-528, 2000.

Schmitke, C., Morency, K., and McPhee J., Using graph theory and symbolic computing to generate efficient models for multi-body vehicle dynamics, *Journal of Multibody Dynamics*, Vol. 222, No. 4, pp. 2041-3068, 2008.

Simpson, A., Fleck, R., Kee, R., Douglas, R., Steele, D., Hanna, A., and Maybin, B., Development of a heavy duty hybrid vehicle model, SAE-2009-01-2933, 2009.

Wei, X., Guzzella, L., Utkin, V.I., and Rizzoni, G., Model-based fuel optimal control of hybrid electric vehicle using variable structure control systems, *Journal of Dynamic Systems, Measurement, and Control*, Vol. 129, No. 1, pp.13-19, 2006.

Wittkopf, A., Automatic code generation and optimization in Maple, *Journal of Numerical Analysis, Industrial and Applied Mathematics*, Vol. 3, pp.167-180, 2008.

Won, J.S., Langary, R., and Ehsani, M., An energy management and charge sustaining strategy for a parallel hybrid vehicle with CVT, *IEEE Trans. On Control Systems Technology*, Vol. 13, No. 2, pp.313-320, 2005.

Wu, B., Mohammed, M., Brigham, D., Elder, R., and White, R.E., A non-isothermal model of a nickel-metal hydride cell, *Journal of Power Sources*, Vol. 101, No. 2, pp.149-157, 2001.

Appendix A: Model Parameters

Table 1. BATTERY PARAMETERS.

Parameters (units)	Symbols	Value
Specific electrode area (cm^2/cm^3)	a_{pos}	4000.0
Specific electrode area (cm^2/cm^3)	a_{neg}	3000.0

Surface area of electrode (cm^2)	A_{pos}	325.0
Surface area of electrode (cm^2)	A_{neg}	360.0
Thickness of electrode (cm)	l_{pos}	3.3×10^{-2}
Thickness of electrode (cm)	l_{neg}	2.8×10^{-2}
Concentration of KOH electrolyte (mol/cm^3)	c_e	7.0×10^{-3}
Reference concentration of KOH electrolyte (mol/cm^3)	$c_{e,ref}$	1.0×10^{-3}
Maximum concentration of Ni(OH)$_2$ in nickel active material (mol/cm^3)	$c_{H^+,max}$	3.7×10^{-2}
Reference concentration of Ni(OH)$_2$ in nickel active material (mol/cm^3)	$c_{H^+,ref}$	$0.5c_{H^+,max}$
Maximum concentration of hydrogen in metal hydride material (mol/cm^3)	$c_{MH,max}$	1.0×10^{-1}
Reference concentration of hydrogen in metal hydride material (mol/cm^3)	$c_{MH,ref}$	$0.5c_{MH,max}$
Exchange current density of reaction at reference reactant concentrations (A/cm^2)	$i_{0,pos,ref}$	1.0×10^{-4}
Exchange current density of reaction at reference reactant concentrations (A/cm^2)	$i_{0,neg,ref}$	1.0×10^{-4}
Reversible heat (V/^{o}K)	$\dfrac{\partial U_{pos}}{\partial T}$	-1.35×10^{-3}
Reversible heat (V/^{o}K)	$\dfrac{\partial U_{neg}}{\partial T}$	-1.55×10^{-3}
Open-circuit voltage (V)	U_{pos}	0.427
Open-circuit voltage (V)	U_{neg}	-0.8279
Internal resistance (Ω)	R_{int}	5.0×10^{-3}
Temperature (^{o}K)	T	298.15

Table 2. VEHICLE PARAMETERS.

Parameters (units)	Value
Vehicle Body	
Body mass (kg)	1380.0
Lumped mass (kg)	10.0
Wheelbase (m)	2.7
Front track (m)	1.524

Rear track (m)	1.519
Tire	
Model	Yokohama Avid S33
Mass (kg)	11.34
Radius (m)	0.349
Width (m)	0.195
Battery Pack	
Number of Ni-MH cells	168
Nominal system voltage (V)	201.6
DC Motor	
Nominal motor power (kW)	60
Nominal armature voltage (V)	650
Nominal motor speed (rpm)	3600
ICE	
Engine volume (L)	1.8
Number of cylinders	4
Engine power (kW)	72 @ 5200 rpm
Bore (mm)	80.5
Stroke (mm)	88.4

Note: For the parameters not listed in Tables 1 and 2, MapleSim default parameters are used.